Midinfrared Resonant Magnetic Nanostructures Exhibiting a Negative Permeability

Shuang Zhang, Wenjun Fan, B. K. Minhas, Andrew Frauenglass, K. J. Malloy, and S. R. J. Brueck*

Center for High Technology Materials, University of New Mexico, Albuquerque, NM 87106, USA

(Received 6 April 2004; published 26 January 2005)

We experimentally demonstrate the first midinfrared (mid-IR) resonant magnetic nanostructures exhibiting a strong magnetic response corresponding to a negative permeability. This result is an important step toward the achievement of a negative refractive index in the IR. The possibility of extending negative permeability to higher frequencies is discussed; a structure with a negative effective permeability at a near-IR resonance frequency of 230 THz (1.3 μm) is proposed.

DOI: 10.1103/PhysRevLett.94.037402 PACS numbers: 78.20.Ci, 42.25.Bs, 42.79.Dj

In 1968, Veselago proposed the concept of a negative refractive index or left-handed material (LHM) [1] with both a negative permittivity (ε) and a negative permeability (μ). Many interesting properties are associated with negative materials including a negative index of refraction, backward phase propagation, a reversed Doppler effect, and backward emission of Cherenkov radiation. Recently, interest in LHMs has increased substantially with the theoretical prediction that a planar slab of LHM functions as a perfect lens without any diffractive loss of resolution [1,2] and with the first demonstrations of LHMs in the rf and THz electromagnetic regions [3–6].

While metals provide a negative permittivity at frequencies below the plasma frequency, naturally occurring materials with negative permeability are not available. Composite electromagnetic materials with resonant structures with sizes much less than the wavelength can act as an effective homogeneous media with a negative permeability. Pendry *et al.* proposed a split ring structure that responds to the magnetic field of incident radiation [7]. The split ring structure (SRS) can be viewed as an equivalent inductor-capacitor (LC) tank circuit. In the presence of a time-varying magnetic field, the magnetic field generated by the current induced in the ring opposes the external magnetic field. At frequencies in the vicinity of the resonance, a negative effective permeability can be realized. While most experimental work has been done at microwave and, more recently, THz frequencies, extending the phenomena to infrared (IR) and visible frequencies will greatly increase the range of applications. Based on the previous modeling work [7] and on the fabrication difficulties associated with scaling the SRS to higher frequency, there has been general pessimism about the prospects of extending these properties to optical frequencies in metallic structures.

In this Letter, we describe the fabrication, characterization, and modeling of arrays of a new nanostructure design with resonances in the mid-IR region and properties that demonstrate strong magnetic activity indicative of negative permeability. To our knowledge, this is the first experimental work on negative permeability reported in the IR. Importantly, the scaling of these results to even higher frequency is investigated, and a structure exhibiting negative permeability in the technologically important near-IR range (1.3 μm) is proposed.

The structure (Fig. 1, top) consists of an array of gold ''staples'' each with two outwardly splayed footings, separated from a thick continuous gold film by a ZnS dielectric layer. Each staple is a LC circuit with the structure part of the inductor associated with the upper loop of the staple and with two capacitors formed between the gold staple footings—the dielectric layer and the bottom gold layer. As a result of the thick Au film, light can only be reflected from or absorbed within the structure; there is no transmission in the IR. For analysis, it is simpler to view this structure in transmission as the staple and its image mir-

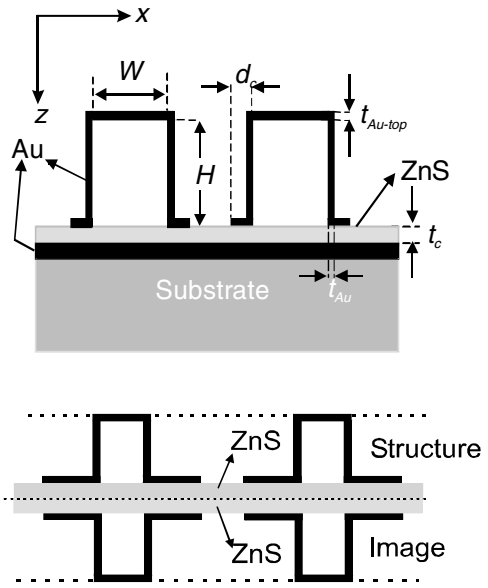

FIG. 1. Top: schematic of the nanostructures. The light is incident from the top; for TM polarization, H is in the y direction, perpendicular to the loop. Bottom: the equivalent LC circuit formed between the top staple structure and its image in the metal. The dashed lines are the reference planes for the effective permeability calculation.

rored in the metal surface, as shown in the bottom panel of Fig. 1. The period of the array is 600 nm, much smaller than the experimentally observed resonant wavelengths of between 4 and 7 μm. The area of the open gold ring loop and the size of the staple footings along with the thickness of the ZnS dielectric determine the inductance and capacitance, respectively, in the equivalent LC circuit. Three 1D samples (magnetic structures extending $\gg\lambda$ into the plane of Fig. 1) (A, B, C) and one 2D structure (as in Fig. 2, extent of each individual structure $\ll\lambda$) [sample (D)] were fabricated with different geometric parameters as shown in Table I. Figure 2 shows SEM micrographs of a 2D structure (D) and a 1D structure (B). Samples A and C have different footing sized (d_c) while samples A and B have different staple heights (H), with all other parameters held constant. Sample D has the same parameters as B except for the periodicity in the y direction and the removal of the nitride inside the loop.

The processing steps for the 1D samples are as follows. First, a 200 nm thick gold film is deposited on a silicon wafer by metal evaporation, followed by dielectric evaporation of a layer of ZnS ($n \sim 2.26$). Zinc sulfide is chosen because it is transparent throughout the $\sim$2 to 10 μm IR region. Next, a layer of Si_3N_4 is grown on the sample by plasma enhanced chemical vapor deposition (PECVD) ($n \sim 1.7$), followed by spun-on layers of a bottom antireflection coating (BARC) and an i-line photoresist (PR). A 1D 600 nm pitch grating is fabricated by interferometric lithography (IL) using a 355 nm, third-harmonic (YAG) laser source [8] [Fig. 3(a) and 3(b)]. The pattern is then transferred into the Si_3N_4 layer by reactive ion etching (RIE) and the residual PR and ARC are removed [Fig. 3(c)]. The etching is selective and does not affect the ZnS layer. Shadow evaporation is used to deposit Au on the top and on one sidewall of the Si_3N_4 gratings, and to form the footing on one side [Fig. 3(d)] of the staples. A second evaporation is carried out at the opposite tilt to form the completed ''staple'' structure. The angle of the metal evaporation controls the footing size. For the 2D samples, the same procedures are followed up to Fig. 3(c), then ARC and PR are spun on the wafer again, and another grating of the same period but perpendicular to the Si_3N_4 grating is fabricated, and further etching and lift-off processes are performed. For these 2D structures, the nitride is removed by plasma ashing after the metal has been deposited.

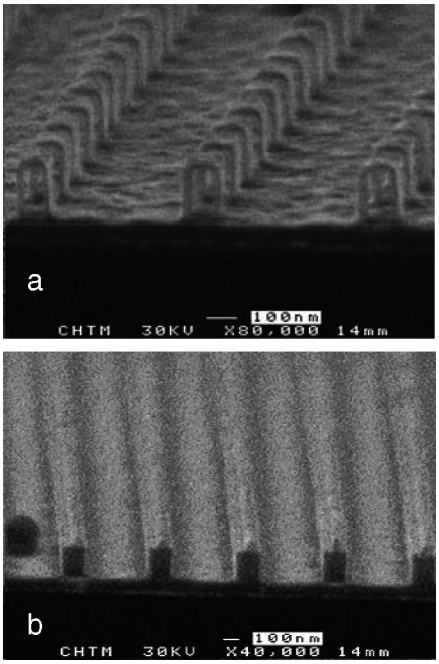

FIG. 2. SEM pictures of the arrays of 2D [sample D, shown in (a)] and 1D [sample B, shown in (b)] staple-shaped nanostructures.

Because of the anisotropic nature of the staple structure, we expect to couple to the resonant structure only when the magnetic field of the incoming light is perpendicular to the loop of the staple (TM polarization). Fourier transform infrared spectroscopy (FTIR) reflectance measurements were performed on these four samples for both TE and TM polarizations. The IR transmission is negligible due to the thick bottom metal, so the nanostructure optical properties are solely characterized by the resonance absorption. As expected, the TE measurements on all the samples did not show any structure [to avoid clutter in the figure, the TE reflectance is shown only for sample C in Fig. 4 (top)]. The TM measurements show reflectance dips that vary according to the sample geometry directly confirming the existence of structure-dependent magnetic activity for these staple arrays. The strong resonance, with as much as 50% absorption in a single layer of nanostructures, suggests that very high fields are generated in the nanostructures that will be of interest for future nonlinear optics experiments. As shown in Fig. 4 (top), sample A has the largest inductance and capacitance, so the resonance occurs at the lowest frequency. Sample C has the same inductance as sample A but a smaller capacitance, giving a higher frequency resonance (shorter wavelength). Samples D and B have the same capacitance as sample A and a smaller inductance, also giving a higher frequency resonance. Comparison between the 1D sample and 2D sample (samples B and D) with the same geometric parameters (not shown) was made; there is no significant difference either in the location of the resonance dip or the depth of the resonance. Experimentally, both samples B and D have relatively smaller reflection dips; the reason for this variation is under investigation.

TABLE I. Sample geometrical parameters (all dimensions in nm).

Sample	W	H	d_c	t_{Au}	$t_{\mathrm{Au\,top}}$	t_c
A	130	280	190	$\sim$15	$\sim$30	80
$B(D)$	130	180	190	$\sim$15	$\sim$30	80
C	130	280	90	$\sim$15	$\sim$30	80
Near-IR	80	50	20	10	20	20

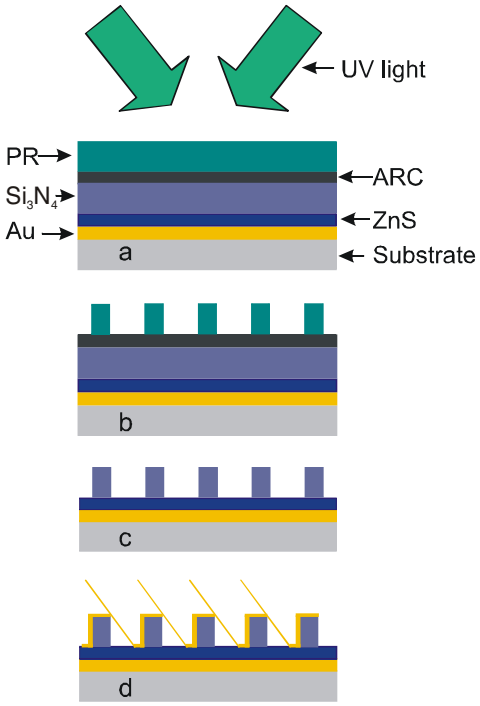

FIG. 3 (color online). Schematic diagrams of fabrication steps. (a) Interferometric lithography with two coherent UV beams. (b) The grating in PR after development. (c) The grating in the nitride layer after RIE etching. (d) Au deposition at an angle from one side.

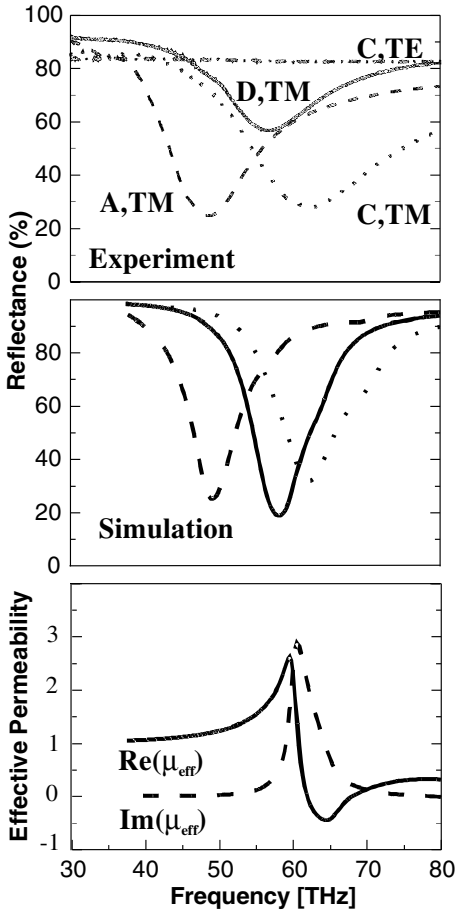

FIG. 4. Experimental (top) and simulation (middle) results for the reflectivity as a function of frequency for three different structures (cf. Table I). The resonance frequency is a function of the nanostructure parameters and is independent of array period, which is the same for all three structures. The resonance is observed only for TM polarization, i.e., incident magnetic field coupled into the inductive structure. The bottom panel shows the effective permeability extracted from the model for sample *C*.

Rigorous coupled wave analysis (RCWA) results for the three 1D structures are shown in Fig. 4 (middle). The RCWA is commonly used for analysis of scattering of electromagnetic waves from periodic structures [9]. Bulk values of the wavelength dependence of the Au optical properties were used [10]. The modeling explains the experimental data well except that the width of absorption dip of the experimental data is somewhat larger than that of the model. The broadening is probably due to the nonuniformity of the structures across the ~1 cm measured spot as well as to the nonideal material parameters.

To further investigate the strength of this magnetic activity, we extracted the effective permeability of sample *C* from the equivalent *LC* circuit (Fig. 1, bottom) [11,12]. The real part of the permeability shows a very strong modulation and is negative over a restricted frequency range; the imaginary part shows a complementary Lorentzian-like peak, features characteristic of a strong magnetic resonance. Extending the modeling across a range of structure parameters shows that a more negative permeability can be obtained by increasing the width *W* of the staple structures, i.e., increasing the fill factor.

Direct scaling of all dimensions of the present structure to extend these results to higher frequency was investigated. The results are shown in Fig. 5. The resonance frequency does not scale linearly with the inverse of the dimensional scaling factor; when the dimensions are reduced by a factor of 4, the resonance only shifts from 70 to 100 THz. At the same time, the minimum permeability becomes positive, evidencing weaker magnetic effects. This is consistent with previous results. Two terms contribute to the inductance: a structural term L_g related to the

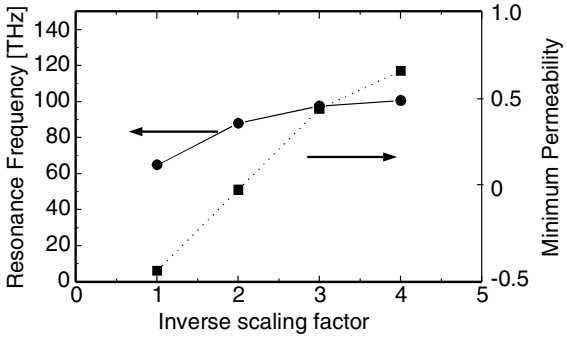

FIG. 5. Scaling of the present structure does not extend negative permeability to significantly higher frequencies as a result of inertial contributions to the structure inductance.

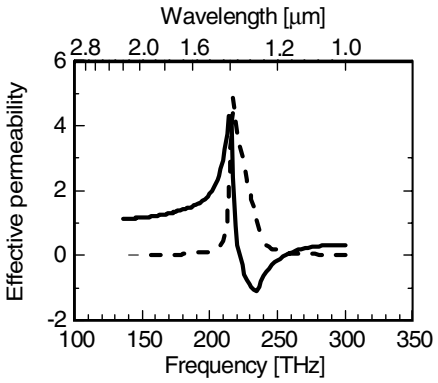

FIG. 6. Simulation of the effective permeability for an optimized structure extending the regime of negative permeability to near-IR wavelengths.

area of the loop, and an intertial term L_i associated with the finite electron mass. L_i is proportional to the circumference of the loop and inversely proportional to the thickness of the metal. The difficulty with simple scaling is the L_i is independent of the scale factor since the effects of reducing the loop perimeter and the metal thickness cancel. Consequently, the inductance and the resonance frequency vary only weakly with dimensional scaling.

The resonance properties of our experimental samples are not yet optimized: the ratio of the linewidth W (130 nm) to the pattern period (600 nm) results in a small fill factor; and the height of the loop H (280 nm) is much larger than W, so the ratio of the area to the perimeter is relatively small, increasing the relative importance of L_i. Increasing W, decreasing H so that $2H \sim W$, and only reducing the metal thickness slightly during the scaling improves the results dramatically. Figure 6 shows the simulated effective permeability for an optimized structure (with dimensions given in the last row of Table I). The pitch is reduced to 180 nm, again small compared to the resonance wavelength of 1.30 μm. The dielectric material was changed to SiO_2 to further decrease the capacitance. The real part of permeability has a strong modulation and a minimum as low as ~ -1 at a frequency of 230 THz (1.3 μm) in the center of the technologically important near-IR spectral region.

In summary, nanostructured magnetic resonators have been fabricated with resonances in the mid-IR spectral region. The measured reflectivity shows an absorption dip in good agreement with the simulation results. The simulation shows strong magnetic response and indicates negative magnetic permeability over a limited frequency range. Scaling to higher frequencies is investigated, and an optimized structure exhibiting strong magnetic resonance behavior at near-IR wavelengths is proposed. Combining this negative permeability structure with a negative permittivity structure will lead to metamaterials with negative refractivity in the IR. This can be accomplished by appropriately modifying the lower metal film, for example, by segmenting it in the orthogonal direction into an array of wires to decrease the effective permittivity [7]. This would also lift the present restriction to reflective operation. The independent control of the magnetic (staple) and electrical (wires) response based on simple geometrical changes will allow tuning of the electromagnetic response over a wide range.

Support for this work was provided by the ARO/MURI in "Deep Subwavelength Optical Nanolithography."

*E-mail address: brueck@chtm.unm.edu

[1] V. G. Veselago, Sov. Phys. Usp. **10**, 509 (1968).
[2] J. B. Pendry, Phys. Rev. Lett. **85**, 3966 (2000).
[3] D. R. Smith, Willier J. Padilla, D. C. Vier, S. C. Nemat-Nasser, and S. Schultz, Phys. Rev. Lett. **84**, 4184 (2000).
[4] R. Shelby, D. R. Smith, and S. Schultz, Science **292**, 77 (2001).
[5] Patanjali V. Parimi, Wentao T. Lu, Plarenta Vodo, and Srinivas Sridhar, Nature (London) **426**, 404 (2003).
[6] T. J. Yen, W. J. Padilla, N. Fang, D. C. Vier, D. R. Smith, J. B. Pendry, D. N. Basov, and X. Zhang, Science **303**, 1494 (2004).
[7] J. B. Pendry, A. J. Holden, D. J. Robbins, and W. J. Stewart, IEEE Trans. Microwave Theory Tech. **47**, 2075 (1999).
[8] X. Chen, S. H. Zaidi, S. R. J. Brueck, and D. J. Devine, J. Vac. Sci. Technol. B **14**, 3339 (1996).
[9] M. G. Moharam and T. K. Gaylord, J. Opt. Soc. Am. **72**, 1385 (1982).
[10] J. H. Weaver, C. Krafka, D. W. Lynch, and E. E. Koch, *Optical Properties of Metals*, Physics Data Vol. I and II (Fachinformationzentrum, Karlsruhe, Germany, 1981), Vol. 18-2.
[11] D. R. Smith and S. Schultz, Phys. Rev. B **65**, 195104 (2002).
[12] S. O'Brien and J. B. Pendry, J. Phys. Condens. Matter **14**, 6383 (2002).